Spectroscopic characterization, docking studies and reactive properties by DFT calculations of halogen substituted 6-Chloro-N-(3-iodo-4-methylphenyl)-pyrazine-2-carboxamide with MD simulations.

P. K. Ranjith[a,b], Angel Ignatious[c], C. Yohannan Panicker[d], B. Sureshkumar[e], Stevan Armakovic[f], Sanja J. Armakovic[g], C. Van Alsenoy[h], P. L. Anto[a,c]*

[a] Department of Physics, Christ College (Autonomous), Irinjalakuda, Thrissur, University of Calicut, Kerala, India

[b] Department of Physics, MPMMSN Trusts College, Shoranur, Palakkad, Kerala, India

[c] Department of Physics, St. Joseph's College (Autonomous), Irinjalakuda, Thrissur, Kerala, India

[d] Thushara, Neethinagar-64, Kollam, Kerala, India

[e] Department of Chemistry, S. N. College, Kollam, Kerala, India

[f] University of Novi Sad, Faculty of Sciences, Department of Physics, Trg D. Obradovica 4, 21000 Novi Sad, Serbia

[g] University of Novi Sad, Faculty of Sciences, Department of Chemistry, Biochemistry and Environmental Protection, Trg D. Obradovica 3, 21000 Novi Sad, Serbia

[h] Department of Chemistry, University of Antwerp, Groenenborgerlaan 171, B-2020, Antwerp, Belgium

* Corresponding author: email address: antoponnore367@gmail.com (P. L. Anto)

Abstract

The spectral characterization of 6-Chloro-N-(3-iodo-4-methylphenyl)-pyrazine-2-carboxamide (CIMPPC) was executed by FT-IR and FT-Raman spectroscopic methods and density functional theory (DFT) computations have been carried using B3LYP/gen method. On the basis of potential energy distribution (PED) the vibrational assignments of the wavenumbers were proposed. NBO analysis was performed to study donor acceptor interactions. Halogen substitution results in increase in the μ (chemical potential) value in comparison with the parent molecule, which is a minimum. Halogen substitution also results a decrease in electrophilicity

index. Fundamental reactive properties of the title molecule is investigated by MEP analysis. Visualization of ALIE and Fukui functions evaluated the most probable sites for electrophilic attacks. Exposure of the title compound towards autoxidation and hydrolysis is evaluated using BDE and RDF. The compatible nature of the compound is investigated through the Hildebrand solubility parameter. CIMPPC exhibit inhibitory activity against the anti-inflammatory receptor transient receptor potential cation channel.

1.   Introduction

To inhibit protein kinases pyrazine products are used extensively, as representatives with antimycotic agent, antiseptic, antineoplastic and anticontagion activities [1]. Pyrazine moieties are found as medical and agricultural drug intermediates and also in a variety of vegetables like bell pepper, beets, asparagus and peanuts, in beef, blackberry, corn, grape fruit juice and breakfast cereal and is mainly used to blend the essence of cocoa, coffee, meat or potato flavor [2]. Pyrazinamide is a member of the pyrazine family and it is known as a very effective antimycobacterial agent, with a well-established role in tuberculosis treatment [3]. Pyrazine carboxamide used for the treatment of tuberculosis as it kills and stops the growth of certain pathogen that cause tuberculosis [4]. Pyrazinoic acid disrupts membrane energetics and inhibits membrane transport function in mycobacterium tuberculosis [5]. Silymarin, a standardized extract of milk thistle seeds also known as Silybium marianum which reduces the dysfunction of liver while maintains the glycemic control [6]. It is an effective antioxidant which prevents the further creation of free radicals by inactivating catalysts, removing the superoxide anion by converting to oxygen and hydrogen peroxide and hinders the lipid synthesis [7,8]. Ubiquitous use of pyrazine in perfume industry, baked food items and in pharmaceutical industry is responsible for the high interest in the compound [9,10]. The family of pyrazine compounds act as photosystem (PS) 2 inhibitors by hindering the photosynthetic electron transport chain in plants, which plays a vital role in ATP production [11−15]. In order to analyze the effect of halogen substitution, in the parent molecule, CIMPPC (26I), the position of iodine atom is replaced by bromine, chlorine and fluorine atoms respectively and which are designated as 26Br, 26Cl, 26F. Similarly the positions of hydrogen atom in the parent molecule CIMPPC, 16H, 18H and 20H are replaced by iodine, bromine, chlorine and fluorine atoms respectively which are

designated as 16I, 16Br, 16Cl, 16F, 18I, 18Br, 18Cl, 18F and 20I, 20Br, 20Cl, 20F. Spectroscopic calculations like FT-IR and FT- Raman were carried out in our compound and also to predict the hardness and stability of the compound we have calculated the Homo-Lumo energy gap. To evaluate the character and reactivity of the compound DFT calculations were carried out. To understand the stability of the title compound when exposed to water surroundings we evaluated the BDE (Bond dissociation energy) and RDF (Radial distribution functions) curves. Solubility parameter is very important in the case of pharmaceutical industry, we have also checked the compatibility of title compound towards the suitable excipient. Due to the vast biological activities of the compound Molecular docking was performed.

2. Experimental Details

The condensation of 6-chloropyrazine-2-carboxylic acid chloride with 3-iodo-4-methylaniline yielded 6-chloro-*N*-(3-iodo-4-methylphenyl)-pyrazine-2-carboxamide [15]. A mixture of 6-chloropyrazine-2-carboxylic acid (50.0 mmol) and thionyl chloride (5.5 mL, 75.0 mmol) in dry toluene (20 mL) was refluxed for about 1 h. Excess of thionyl chloride was removed by repeated evaporation with dry toluene *in vacuo*. The crude acyl chloride dissolved in dry acetone (50 mL) was added dropwise to a stirred solution of the 3-iodo-4-methylaniline (50.0 mmol) in 50 mL of dry pyridine at room temperature. After the addition was complete, stirring continued for another 30 min. The reaction mixture was then poured into 100 mL of cold water and the crude amide was collected and recrystallized from aqueous ethanol (scheme 1).

2.1   6-Chloro-N-(3-iodo-4-methylphenyl)-pyrazine-2-carboxamide (CAS Registry Number: 1072927-31-1).

Yield 83%; Anal. Calcd. For $C_{12}H_9ClIN_3O$ (373.6): 38.58% C, 2.43% H, 11.25% N; Found: 38.80% C, 2.62% H, 11.37% N. Mp 173.4-174.5 °C; Log *P*: 3.33; Clog *P*: 3.54369; TLC: *R*F = 0.81; 1H-NMR δ: 9.38 (1H, s, H3), 9.32 (1H, bs, NH), 8.81 (1H, s, H5), 8.21 (1H, d, *J*=2.2 Hz, H2´), 7.68 (1H, dd, *J*=8.2 Hz, *J*=2.2 Hz, H6´), and 7.24 (1H, d, *J*=8.2 Hz, H5´), 2.42 (3H, s, CH3); 13C-NMR δ: 159.2, 147.6, 147.4, 143.7, 142.2, 138.3, 135.3, 129.9, 129.7, 119.8, 100.8, and 27.5.
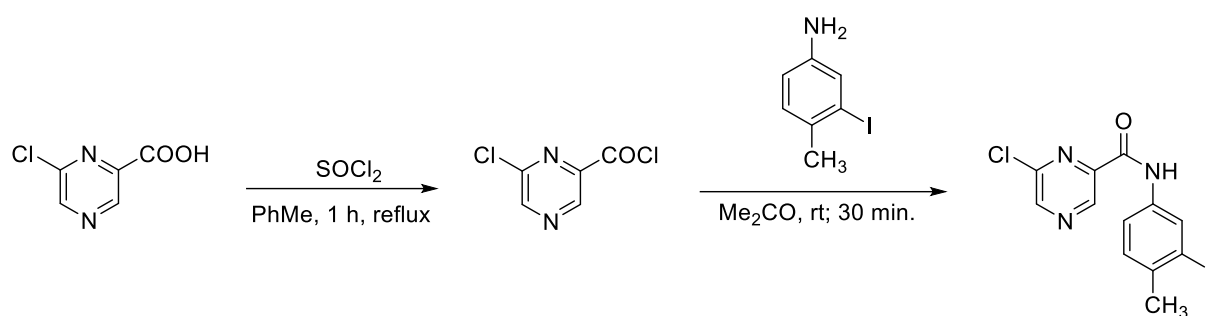
Scheme 1. Preparation of the target compound

Pyrazine derivatives have been synthesized and successfully evaluated as agents with diverse pharmacological effects, including but not limited to antiproliferative, antiinfective, and effects on cardiovascular or nervous system, and some of them have become clinically used drugs worldwide [16]. Pyrazinamide (PZA), a first-line anti-TB drug, was discovered through an effort to find antitubercular nicotinamide derivatives. Our research is focused on PZA analogues with a -CONH- bridge connecting the pyrazine and benzene rings. This moiety can form centrosymmetric dimer pairs with the peptidic carboxamido group of some peptides, needed for binding to the receptor site, possibly by formation of hydrogen bonds. 6-Chloro-*N*-(3-iodo-4-methylphenyl)-pyrazine-2-carboxamide had minimal antimycobacterial activity (MIC = 8 mg/L) against M. tuberculosis comparable with the standard PZA (MIC = 8 mg/L) [17]. The photosynthesis inhibition, antialgal activity and the effect of a series of pyrazine derivatives as abiotic elicitors on the accumulation of flavonoids in a callus culture of Ononis arvensis (L.) were investigated and the most active inhibitor of the oxygen evolution rate in spinach chloroplasts was 6-Chloro-*N*-(3-iodo-4-methylphenyl)-pyrazine-2-carboxamide (IC_{50} = 51.0 µmol/L). The maximal flavonoid production (about 900%) was reached after a twelve-hour elicitation process with 6-Chloro-*N*-(3-iodo-4-methylphenyl)-pyrazine-2-carboxamide [15]. The FT-IR spectrum was recorded using KBr pellets on a DR/JASCO FT-IR 6300 spectrometer. The FT-Raman spectrum was obtained on a Bruker RFS 100/s, Germany. For excitation of the spectrum, the emission of Nd:YAG laser was used with an excitation wavelength of 1064 nm, a maximal power 150 mW; measurement of solid sample.

3. Computational Details

Calculations of the title compound were carried with using the Gaussian09 program [18] using the B3LYP method, gen basis set for C, H, N, O atoms and LANL2DZ basis set for iodine atom to predict the molecular structure and wavenumbers in the gaseous phase and a scaling factor of 0.9613 had to be used for obtaining a considerably better agreement with the experimental data [19]. The assignments of the calculated wavenumbers are done using GAR2PED [20] and GaussView software [21]. DFT calculations were performed using Jaguar 9.0 program [22]. While MD simulations were carried out using Desmond program [23]. Using Jaguar program DFT calculations were carried out using B3LYP exchange-correlation functional, with 6-311++G(d,p), 6-31+ G(d,p) and 6-311G(d,p) basis sets for the calculations of ALIE, Fukui functions, BDE and RDF respectIvely. In case of MD simulations the OPLS 2005 force field has been employed with simulation time set to 10 ns within isothermal- isobaric (NPT) ensemble class [24]. For MD simulations system was modeled by placing one CIMPPC molecule into the cubic box with ~3000 water molecules. Other parameters include temperature of 300 K, pressure of 1.0325 bar and cut off radius of 12 Å. Schrödinger Materials Science Suite 2015-4 was used, Maestro GUI [25] was used for the preparation of input files and analysis of results.

4. Results and Discussion

In the following discussion, phenyl and pyrazine rings are designated as Ph and Pz respectively.

4.1 Optimized geometrical parameters

The C-N and C-C bond lengths in the pyrazine ring of the title compound are 1.3318, 1.3394, 1.3440, 1.3185 Å and 1.3971, 1.4038 Å, respectively, which are shorter than the normal C-N bond length (1.4900 Å) and the C-C bond length (1.5400 Å). The reported C-N and C-C bond lengths of the pyrazine ring are 1.4104, 1.3577, 1.3577, 1.3608 Å and 1.4121, 1.3517 Å [26]. The bond lengths C_9-N_{11} and C_{12}-N_{11} (the carboxamide linker) are 1.3657 Å and 1.4074 Å which are also shorter than the normal C-N single bond and these bonds have some character of a double or conjugated bond [27]. The C-C bond lengths in the phenyl ring are in the range 1.3890-1.4043Å. At N_{11} and C_{17} positions, the bond angles C_9-N_{11}-H_{21}, C_9-N_{11}-C_{12}, C_{12}-N_{11}-H_{21} and C_{14}-C_{17}-I_{26}, C_{19}-C_{17}-I_{26}, C_{14}-C_{17}-C_{19} are 114.3°, 128.8°, 116.9° and 116.4, 120.2 and 123.4°

respectively. These asymmetries of angles are due to the weakening of the N-H bond and iodine substitution in the phenyl ring respectively. The bond angles C_4-C_5-N_6, C_4-C_5-C_9, C_9-C_5-N_6 at C_5 are 121.2, 120.0 and 118.8° respectively. This asymmetry is attributed to the interaction of pyrazine ring and carboxamide group. The bond angles C_{17}-C_{19}-C_{22}, C_{15}-C_{19}-C_{22}, C_{17}-C_{19}-C_{15} at C_{19} are 123.9, 120.2, 115.9° and the asymmetry is due to the interaction of the neighboring groups.

4.2   IR and Raman Spectra

The calculated wavenumbers, observed Raman, IR bands and the assignments are given in Table 2. According to literature, the NH vibrations are expected in the region, 3390 ± 60 cm^{-1} (stretching), in the range 1500-1200 and in the region 790 ± 70 cm^{-1} (bending modes) [28-31]. For the title compound, these modes were assigned at 3330 cm^{-1} (IR), 3494 cm^{-1} (Raman), 3418 cm^{-1} (DFT) (stretching), 1509 cm^{-1} (DFT) (in-plane bending), 674 (IR), 668 (Raman), 667 cm^{-1} (DFT) (out-of-plane bending). For the title compound, the NH stretching mode has an IR intensity of 76.90 and Raman activity of 247.15 with a PED of 91%. The PED of NH deformation modes of the title compound are in between 34 and 44%. For the deformation mode at 667 cm^{-1}, the IR intensity is low while the other mode has high IR intensity for the title compound. In the present case, the NH stretching mode is red shifted by 88 cm^{-1} in the IR spectrum from the computed value, which indicates the weakening of the NH bond [32]. The CN stretching modes are expected in the region 1275 ± 55 cm^{-1} [28] and the bands at 1232 cm^{-1} (DFT) with low IR intensity and PED around 28%, at 1230 cm^{-1} (IR) spectrum and 1237 cm^{-1} (Raman) spectrum are assigned as the CN stretching modes of the title compound. The reported CN stretching modes are at 1265, 1239 cm^{-1} in the IR spectrum and at 1261, 1248 cm^{-1} (DFT) [33]. For the title compound, the carbonyl stretching vibration is observed at 1670 cm^{-1} in the IR spectrum and at 1667 cm^{-1} in the Raman spectrum which is expected in the region 1715-1600 cm^{-1} [28], while the computed value is 1706 cm^{-1} with an IR intensity of 198.96 and Raman activity 153.36 and the PED is 66%. According to literature [28], the CH$_3$ modes are expected in the regions 3050-2900 cm^{-1} (stretching), 1485-1350, 1100-900 cm^{-1} (deformation modes) and for the title compound, these modes are assigned at 3024, 2982, 2925 cm^{-1} (IR), 2957, 2924 cm^{-1} (Raman), 3010, 2987, 2934 cm^{-1} (DFT) (stretching), 1433, 1031 cm^{-1} (IR), 1035 cm^{-1} (Raman) and in between 1462-989 cm^{-1} (DFT) (bending). Analysis of vibrational spectra of substituted benzenes shows that the stretching vibrations of CI corresponds to a band around 340 cm^{-1} experimentally [34,35]. The carbon-iodine stretching band of the title compound is assigned at 311 cm^{-1}

theoretically, 271 cm^{-1} experimentally. Zainuri et al. reported the CI stretching mode at 317 cm^{-1} [36]. For the title compound, the phenyl CH stretching bands are observed at 3062 cm^{-1} in the IR spectrum and 3063 cm^{-1} in the Raman spectrum, while the computed values are in the range 3159-3059 cm^{-1} which are in agreement with the literature [28,37]. The phenyl ring stretching modes of the title compound are observed at 1580, 1485, 1298 cm^{-1} in the IR spectrum, at 1598, 1561, 1302 cm^{-1} in the Raman spectrum and at 1596, 1571,1476, 1373, 1291 cm^{-1} theoretically (DFT) [29]. The tri-substituted phenyl ring breathing mode of the title compound is assigned at 862 cm^{-1} (IR), 866 cm^{-1} (Raman) and 858 cm^{-1} (DFT) with PED 21% which is in agreement with the literature [38]. The in-plane and out-of-plane CH deformations of the phenyl ring are expected above and below 1000 cm^{-1} respectively [28] and these modes of the title compound were assigned at 1269, 1248, 1193 cm^{-1} (DFT), 1166, 926 cm^{-1} (IR), 1179 (Raman) (in-plane bending modes), 908, 890, 794 cm^{-1} (DFT) (out-of-plane bending modes). The IR bands in the region of 2676-1800 cm^{-1} and the large broadening seen in the IR spectrum support the intra-molecular hydrogen bonding [39]. The pyrazine CH stretching modes of the title compound were observed at 3116, 3093 cm^{-1} theoretically which are expected in the range 3100-3000 cm^{-1} [40]. In the present case, the pyrazine ring stretching modes were observed at 1520, 1121 cm^{-1} in the IR spectrum and at 1525, 1395, 1118 cm^{-1} in the Raman spectrum while the PED analysis gives these modes in a range 1548-1145 cm^{-1} which are in agreement with literature [2,33]. In the present case, the pyrazine ring stretching modes have IR intensities in the range 2.18 to 59.64 and Raman activities 6.05 to 477.37 and the PEDs are around 50%. For the title compound, the ring breathing mode of the pyrazine ring was assigned at 991 cm^{-1} in the DFT with low IR intensity and Raman activity, while the reported value is at 1015 cm^{-1} (DFT) [2]. For the title compound, the in-plane and out-of-plane CH bending modes of the pyrazine ring were assigned at 1384, 1158, 943 and 884 cm^{-1} theoretically. The experimentally observed values are 1147, 958 cm^{-1} which are in agreement with the literature [2].

4.3   Natural Bond Orbital Analysis

The NBO (Natural Bond Orbital) calculations were performed using NBO 3.1 program [41]. The important interactions are: LPCl$_{27}$→C$_1$-N$_6$, LPN$_{11}$→C$_{12}$-C$_{13}$, LPN$_{11}$→C$_9$-O$_{10}$, LPO$_{10}$→C$_9$-N$_{11}$, LPO$_{10}$→C$_5$-C$_9$, C$_{15}$-C$_{19}$→C$_{14}$-C$_{17}$ and C$_{15}$-C$_{19}$→C$_{12}$-C$_{13}$ with energies, 14.26, 31.00, 50.74, 22.46, 18.84, 23.23 and 22.77 kcal/mol. 100% p-character is found in Cl$_{27}$, I$_{26}$, N$_{11}$ and O$_{10}$. The NBO interactions are tabulated in Tables 3 and 4.

4.4   Nonlinear optical properties

The calculated first hyperpolarizability of the title compound is 24.973×10^{-30} esu which is 192.1 times that of standard NLO material urea (0.13×10^{-30} esu) [42]. For a pyrazine derivative the first hyperpolarizability is reported at 9.77×10^{-30} esu [26]. We conclude that the title compound is an attractive object for future studies of nonlinear optical properties. In CIMPPC halogen substitution increases the dipole moment in the order 26>18>16>20. Highest dipole moment value is noticed for 26Cl and lowest value for 20I. Highest polarizability (α) value is noticed for 20I and lowest value for 18I. For first order hyperpolarizability, β value decreased to a large extent for 18th position for F, Cl and I except Br. Highest β value is noticed for 20I and lowest value for 18Cl.

4.5   Frontier Molecular Orbitals

In order to understand global stability and reactive properties of the title compound we have investigated frontier molecular orbitals. Namely, the highest occupied molecular orbital (HOMO) and lowest unoccupied molecular orbital (LUMO) are the main molecular orbitals that take part in reactions with other molecular structures. Distribution of HOMO and LUMO provides important insight into the reactive properties of organic molecules. The HOMO-LUMO visualization is represented in Fig. 4. Frontier molecular orbital study is used to explain the chemical behaviour and stability of the molecular system. The delocalization of HOMO and LUMO over the molecular system shows the charge transfer within the molecular system. The HOMO-LUMO gap for the title compound is found to be 0.834eV. The chemical descriptors can be evaluated by using HOMO and LUMO orbital energies, E_{HOMO} and E_{LUMO} as: ionization energy $I = -E_{HOMO}$, electron affinity $A = -E_{LUMO}$, hardness $\eta = (I-A)/2$, chemical potential $\mu = -(I+A)/2$ and electrophilicity index $\omega = \mu2/2\eta$ [43]. For the title compound, $I = 5.934$, $A = 5.100$, $\eta = 0.417$, $\mu = -5.517$ and $\omega = 36.496$eV. For the title compound the HOMO is delocalized over the entire iodine atom and slightly over the phenyl ring and CH_3 group while the LUMO is delocalized over the entire molecule except iodine, chlorine atom and CH_3 group. For halogen substitution 26Br, HOMO is delocalized only over the pyrazine ring. For 26Cl substitution HOMO is delocalized over the entire molecule except the C=O group and the nitrogen atom (position 3) of pyrazine ring. For 26F HOMO is over entire pyrazine ring except nitrogen (position 3). While for 26Br, 26Cl and 26F the LUMO delocalization is same over the entire molecule except the CH_3 group, chlorine atom and corresponding halogen atoms. For halogen

substitution 16I HOMO is delocalized the entire phenyl ring and iodine atom. For 16Br the HOMO is over entire pyrazine ring except nitrogen atom (position 3). For 16Cl HOMO is delocalized entire phenyl ring, C=O group and slightly over the pyrazine ring. For 16F the HOMO is delocalized over entire pyrazine ring except nitrogen atom (positon 3) and slightly over the phenyl ring and nitrogen atom of carboxamide group. For halogen substitution 16I, 16Br, 16Cl and 16F the LUMO delocalization is the same over the entire molecule except the CH_3 group, chlorine atom and the corresponding halogen atoms and this is also as in the previous halogen substitutions. For halogen substitutions 18I the HOMO is strongly delocalized over the iodine atom. For halogen substitution 18Br the HOMO is over entire pyrazine ring except nitrogen atom (Position 3). For 18Cl substitution the HOMO is delocalized strongly over the entire phenyl ring and slightly over the pyrazine ring and carboxamide group. For halogen substitution 18F the HOMO is delocalized over entire pyrazine ring. For halogen substitutions 18I and 18F the LUMO is localized same over entire pyrazine ring and carboxamide group. Similarly for halogen substitutions 18Br and 18Cl the LUMO delocalization is strong over entire pyrazine ring except chlorine atoms. For halogen substitution 20I the HOMO is delocalized strongly around the iodine atom. For the halogen substitutions 20Br and 20F the HOMO is delocalized strongly over the entire pyrazine ring except the nitrogen atom (Position 3). For halogen substitution 20Cl the HOMO is strongly delocalized over entire pyrazine ring except nitrogen atom (position 3) and also substituted chlorine atom and partially over phenyl ring. For 20I and 20Cl the LUMO is delocalized strongly over the pyrazine ring except chlorine atom and slightly over carboxamide and phenyl group. For halogen substitution 20Br the LUMO is over entire molecule except CH_3 group, bromine and chlorine atoms. For halogen substitution 20F, LUMO is delocalized over the entire pyrazine ring except chlorine atom, slightly over carboxamide group and phenyl ring. The average value of chemical potential decreases for the halogen substitution in the order 26I, 16I, 18I, 20I less than 26Cl, 16Cl, 18Cl, 20Cl less than 26F, 16F, 18F, 20F less than 26Br, 16Br, 18Br, 20Br. Chemical potential value of 16Br is deviated maximum from the parent molecule while all other halogen substitution shows considerable deviation. Halogen substitution results in increase in the μ value in comparison with the parent molecule, which is a minimum. Halogen substitution also results a decrease in electrophilicity index and is minimum for 18Br. Global hardness is higher for 18Br because of its large HOMO-LUMO gap which results a decrease in polarizability

4.6 Molecular Electrostatic Potential Map

Molecular electrostatic potential and electron density are related to each other to find the reactive sites for electrophilic and nucleophilic sites [44,45]. The negative (red and yellow) regions of MEP map were related to electrophilic reactivity while the positive (blue) regions to nucleophilic reactivity. For the parent molecule, most electrophilic (red and yellow) regions are around C=O of carboxamide group, deeply over entire phenyl ring, and slightly near nitrogen atom (position 3) and the nucleophilic regions (blue) are deeply over iodine atom and slightly over the pyrazine ring (Fig. 5). For halogen substitutions 26Br, 26Cl, 26F, the electrophilic regions are strongly over the C=O group of carboxamide, slightly over the phenyl ring and nitrogen atom (position 3) while the nucleophilic regions are over the N-H of carboxamide group and the pyrazine ring but the blue region deeply over pyrazine ring in 26Br is more pronounced. For iodine substitution in 16I the electrophilic regions are around C=O of carboxamide group, deeply over phenyl ring and slightly near N-H bond and the blue region is deeply over iodine atom and pyrazine ring. For halogen substitution 16Br, the electrophilic regions are at C=O region, slightly over phenyl ring and deeply over N-H bond. For chlorine and fluorine substitution 16Cl, 16F the electrophilic regions are similar to that of bromine substitution while the nucleophilic regions are similar to that of bromine substitution but blue region of chlorine atom in 16Cl is more pronounced. For halogen substitutions 18Br, 18Cl, 18F the electrophilic behavior is around C=O and slightly over phenyl ring is identical to that of 18I where red region is slightly over nitrogen atom (position 3) while the nucleophilic region is identical to that of 18I. For the halogen substitutions 20Br, 20Cl and 20F the red region is over C=O, slightly over phenyl ring and near nitrogen atom (position 3) while the blue region is near N-H bond and over pyrazine ring. For halogen substitution 20I the electrophilic region is deeply over C=O, entire phenyl ring and near nitrogen atom (position 3) while the nucleophilic region is deeply over iodine atom and around pyrazine ring.

4.7 ALIE surfaces and Fukui functions

ALIE (Average local ionization energy) is a quantum molecular descriptor which indicates the local reactivity and also the energy required to remove an electron from the molecule. So we can say that the sites with least values of ALIE are the most probable sites for an electrophilic attack [46,47]. According to the equation given below ALIE is the sum of orbital energies weighted by the orbital density.

$$I(r) = \sum_i \frac{\rho_i(\vec{r})|\varepsilon_i|}{\rho(\vec{r})}$$

Where $\rho_i(\vec{r})$ denotes electronic density of the i-th molecular orbital at the point $\vec{r}$, ε_i denotes orbital energy and $\rho(\vec{r})$ denotes total electronic density function. We have mapped the ALIE values to the electron density surface in order to foresee the attacking sites of electrophiles. The ALIE figure is represented in Fig. 6. Here in this figure we can see that the Iodine atom and benzene ring shows the least ALIE values that is 179.47 kcal/mol. On the other side in the close vicinity of hydrogen atoms H_{24}, H_{21}, H_8, H_7 the highest ALIE value 332.15 kcal/mol is visible. The functional derivative of chemical potential with respect to external potential is termed as Fukui functions. It is also used to predict the reactivity sites. When we go through the maxwell's relations we can interpret this as the derivative of electronic density with respect to the number of electrons [48,49]. In physical sense it is the change in electron density as a consequence of change in charge. These functions in Jaguar program are calculated with the help of finite difference approach, according to the following equations:

$$f^+ = \frac{\left(\rho^{N+\delta}(r) - \rho^N(r)\right)}{\delta},$$

$$f^- = \frac{\left(\rho^{N-\delta}(r) - \rho^N(r)\right)}{\delta},$$

where N stands for the number of electrons in reference state of the molecule, while δ stands for the fraction of electron which default value is set to be 0.01 [50]. By plotting fukui functions to electron density surfaces we get a convenient information about the important molecular sites acting as a reactive center [46,47]. The Fukui function plot is represented in Fig. 7. The colour coding in the plot is as follows, purple (positive) colour in Fukui function f^+ means the electron density has been increased by the addition of charges to the system while red (negative) colour in Fukui function f^- means the electron density has been diminished by the addition of charges. Electron density is increased in the near vicinity of carbon atoms C_{12}, C_{22}, C_{17} and electron density is decreased near the Cl_{27} atom.

4.8   Reactive and degradation properties based on autoxidation and hydrolysis

BDEs and RDFs are calculated to predict degradation properties based on autoxidation and hydrolysis mechanisms. Calculations of BDE for hydrogen abstraction allow the possibility to

predict molecular sites where autoxidation process could start. It gives information about upto what extent some molecule are sensitive to presence of oxygen and open air, a parameter that is of very much importance in pharmaceutical industry. BDE also helps us to understand the forced degradation studies, since they can be used for confirmation and determination of degradation path of some organic pharmaceutical molecule [51-54]. Wright et al. says that the target molecule is most vulnerable to autoxidation if the BDE for hydrogen abstraction ranges from 70 to 85 kcal/mol [55]. BDE values for hydrogen abstraction lower than 70 kcal/mol, are not suitable for the autoxidation mechanism since formed radicals are resistant for O_2 insertion [55-57]. Fig.8 contains all BDE values for CIMPPC. Red colored values represent the BDE values for hydrogen abstraction and blue colored values correspond to the BDE values for the rest of the single acyclic bonds. All the BDE values of molecule are greater than 90 kcal/mol so we can say that the molecule is stable in the presence of oxygen and open air. To find the extend of hydrolysis we have also calculated the RDF for the molecule. In fig.9 RDFs of atoms with the most pronounced interactions with water molecules are presented. In RDF plot, $g(r)$ represents the probability of finding a particle in the distance r from another particle [58]. Results provided in Fig.9 indicate that only four atoms of CIMPPC molecule have relatively significant interactions with water molecules. These atoms are C_{22}, O_{10}, I_{26} and Cl_{27} which shows similar g(r) profile. Peak distance in all cases is located between 2.9 to 3.9 Å. According to the maximal g(r) values the most important RDF is certainly for chlorine atom. Here the high peak and absence of hydrogen atoms indicates the possibility of the stability of molecule in water surroundings which is a very important property in the pharmaceutical industry

4.9   Solubility parameter

The production of new pharmaceutical care products and the identification of the active ingredient are emerging fields. There are certain parameters to be satisfied by the molecules for considering the drug production. Some of them are stability, solubility and deliverability of the active ingredient. The molecules which lack these physical properties must be modified. By mixing them with the excipient we can modify the active ingredient without any structural changes. A wide range of excipients are identified over the past decade. Excipients can be identified using experimental as well as computational methods. Experimental identification is a very time consuming process, while computational methods can be used to neutralize the

possibilities. Compatibility is one of the major property needed between the active ingredient and the excipient. Hildebrand solubility parameter can be used to predict the compatible nature of both [59-61]. The solubility parameter of active component and that of the excipient must be same. The equation for the solubility parameter using MD calculations is given below

$$\delta = \sqrt{\frac{\Delta H_V - RT}{V_m}}$$

In this work, the solubility parameter has been calculated for the CIMPPC molecule. The value is compared with three compounds polyvinylpyrrolidone polymer (PVP), maltose, and sorbitol. MD systems used to calculate this quantity consisted of 32 molecules placed in a cubic simulation box. Solubility parameters of all mentioned compounds have been summarized in Table 7. As indicated by the results presented in Table 7, CIMPPC molecule has the highest compatibility with the Maltose compound. In this particular case, the difference between corresponding values of solubility parameter is less than 5.5 MPa$^{1/2}$, indicating very high compatibility. Solubility parameter of sorbitol is much higher than the solubility parameter of the CIMPPC molecule. Therefore, the MD calculations suggest that it is reasonable to consider Maltose as an excipient for CIMPPC molecule.

4.10   Molecular docking

Molecular docking was employed to recognize the active site of the receptor, and acquire the best geometry of ligand-receptor complex. Based on the structure of a compound, PASS (Prediction of Activity Spectra) [62] is an online tool which predicts different types of activities. We choose the activity Vanilloid 1 agonist with Pa value 0.708 and high resolution crystal structure of corresponding protein transient receptor potential cation channel (PDB ID: 4DX1) was downloaded from the RCSB protein data bank website. Transient receptor potential vanilloid 1 (TRPV1), a non-selective cation channel. TRPV1 is thought to be a central transducer of hyperalgesia and a prime target for controlling pain pharmacologically because it is a point where many proalgesic pathways converge and it is upregulated and sensitized by inflammation and injury [63]. A novel transient receptor potential vanilloid 1 (TRPV1) agonist inhibits TNF-alpha production through the activation of capsaicin-sensitive afferent neurons and treatment of chronic inflammation [64]. Pharmacologically active pyrazine N-acylhydrazone (NAH) derivatives, is used as novel analgestic and anti-inflammatory drug candidates [65]. Thus we choose title compound as ligand and transient receptor potential cation channel as target for docking study.

All molecular docking calculations were performed on AutoDock4.2 [66] and Auto Dock-Vina software [67]. The original ligands as well as water molecules were removed from the crystal structure and polar hydrogens and united atom Kollman charges were assigned for the receptor using the graphical user interface Auto Dock Tools (ADT). The Lammarckian Genetic Algorithm (LGA) [68] was employed to calculate the energy between ligand and receptor. The compound docked the active site of receptors with the grid centre dimension 40×40×40. The conformations with the lowest binding energy is extracted and analyzed for detailed interactions in Discovery Studio Visualizer 4.0 software. The ligand binds at the active site of the substrates by weak non-covalent interactions (Fig.10 and Fig. 11). The amino acid Arg186 forms two H-bond with carbonyl group while Thr190 has a H-bond with NH group. Pro230 having a H-bond with pyrazine ring. The docked ligand forms a stable complex with transient receptor potential cation channel and the binding free energy value is -5.9 kcal/mol (Table 9). These preliminary results suggest that the compound having inhibitory activity against the anti-inflammatory receptor transient receptor potential cation channel. Thus the title compound can be developed as drug used for the treatment of pain and inflammation.

5. Conclusion

FT-IR and FT Raman spectra of 6-chloro-N-(3-iodo-4 methyl phenyl) pyrazine-2-carboxamide were recorded and analyzed. The vibrational wavenumbers were computed at B3LYP theory. The data obtained from theoretical calculation are used to assign vibrational band obtained experimentally. The geometrical parameters of the title compound are in agreement with similar derivatives. For the title compound the HOMO is delocalized over the entire iodine atom and LUMO is delocalized over the entire except iodine atom also halogen substituted HOMO-LUMO calculations are conducted the lowering of HOMO-LUMO band gap support the bioactive property of the molecule. The molecular electrostatic potential study showed that for the parent molecule most electrophilic regions are around C=O of carboxamide group and the nucleophilic region deeply over iodine atom. The NBO analysis performed in this study enabled us to know about the conjugate interactions taking place within the molecular spices. The calculated first hyperpolarizability of the title compound is 192.1 times that of standard NLO material, which is suitable for non-linear optical activity. By DFT calculations we were able to calculate the ALIE values, beside benzene ring and iodine atom we have determined H_{24}, H_{21}, H_8, H_7 are prone to electrophilic attacks. The

mapping of Fukui functions against electron density shows that carbon atoms C_{12}, C_{22}, C_{17} and chlorine atom Cl_{27} are important reactive centers. Calculation of BDE and RDF showed that title molecule is not sensitive in the water surroundings towards auto oxidation and degradation mechanisms. The MD calculations of solubility parameter suggests that it is reasonable to consider Maltose as an excipient for CIMPPC molecule. By molecular docking the compound forms a stable complex with Transient receptor potential vanilloid 1 (TRPV1).

Acknowledgments

References

[1]   D. R. Boubee, C. V. Leeuwen, D. Dubourdieu, Organoleptic impact of 2-methoxy-3-isobutylpyrazine on red brodeaux and loire wines, effect of environmental conditions on concentrations in grapes during ripening, J. Agric. Food Chem. 48 (2000) 4830-4834.

[2]   H. Endredi, F. Billes, S. Holly, Vibrational spectroscopic and quantum chemical study of chlorine substitution of pyrazine, J. Mol. Struct. Theochem. 633 (2003) 73-82.

[3]   A. Somoskovi, M. M. Wade, Z. Sun, Y. Zhang, Iron enhances the antituberculous activity of pyrazinamide, J. Antimicrob. Chemother. 53 (2004) 192-196.

[4]   V. Opletalova, Jirı. Hartl, A. Patel, K. Palat Jr., V. Buchta, Ring substituted 3-phenyl-1-(2-pyrazinyl)-2-propen-1-ones as potential photosynthesis-inhibiting, antifungal and antimycobacterial agents, Il Farmaco 57 (2002) 135-144.

[5]   Y. Zhang, M. M. Wade, A. Scorpio, H. Zhang Z. Sun, Mode of action of pyrazinamide: disruption of Mycobacterium tuberculosis membrane transport and energetics by pyrazinoic acid J. of Antimicrob. Chemother. 52 (2003) 790-795.

[6]   V. Křen, D. Walterova, Silybin and silymarin–New effects and applications. Biomed. Pap. 149 (2005) 29-41.

[7]   S. S. Raza, M. M. Khan, M. Ashafaq, A. Ahmad, G. Khuwaja, A. Khan, Silymarin protects neurons from oxidative stress associated damages in focal cerebral ischemia: A

behavioral, biochemical and immune histological study in Wistar rats. J. Neurol. Sci. 309 (2011) 45-54.

[8]. N. K. Singhal, G. Srivastava, D. K. Patel, S. K. Jain, M. P. Singh, Melatonin or silymarin reduces maneb- and paraquat-induced Parkinson's disease phenotype in the mouse. J. Pineal Res. 50 (2011) 97-109.

[9] W. J. Chung, A. Kornilov, B. H Brodsky, M. Higgins, T. Sanchez, L. B. Heifets,. M. H. Cynamon, J. Welch, Inhibition of M. tuberculosis in vitro in monocytes and in mice by aminomethylene pyrazinamide analogs. Tuberculosis 88 (2008) 410-419.

[10] B. Servusová, D. Eibinová, M. Doležal, V. Kubícek, P. Paterová, M. Peško, Substituted N-benzylpyrazine-2-carboxamides: Synthesis and biological evaluation, Molecules 17 (2012) 13183-13198.

[11] D. M. Kráľová, K. Herbicides, Theory and Applications: Synthesis and Evaluation of Pyrazine Derivatives with Herbicidal Activity. In Tech; 2011.

[12] M. Doležal, K. Kráľová, Synthesis and Evaluation of Pyrazine Derivatives with Herbicidal Activity. In Herbicides, Theory and Applications; S Soloneski, M.L. Larramendy, Eds.; In Tech: Vienna, Austria, (2011) 581-610.

[13] M. Dolezal, J. Zitko, Z. Osicka, J. Kunes, M. Vejsova, V. Buchta, J. Dohnal, J. Jampilek, K. Kralova, Synthesis, antimycobacterial, antifungal and photosynthesis-inhibiting activity of chlorinated N-phenylpyrazine-2-carboxamides. Molecules 15 (2010) 8567-8581.

[14] M. Dolezal, P. Cmedlova, L. Palek, J. Vinsova, J. Kunes, V. Buchta, J. Jampilek, K Kralova, Synthesis and antimycobacterial evaluation of substituted pyrazine carboxamides. Eur. J. Med. Chem. 43 (2008) 1105-1113.

[15] M. Doležal, L. Tumová, D. Kešetovičová, J. Tuma, K. Kráľová, Substituted N-phenylpyrazine-2-carboxamides, their synthesis and evaluation as herbicides and abiotic elicitors. Molecules 12 (2007) 2589-2598.

[16] M. Dolezal, J. Zitko, Pyrazines Derivatives: a patent review (June 2012-present). Exp. Opin. Ther. Pat., 25 (2015) 33-47.

[17] M. Dolezal, J. Zitko, D. Kesetovicova, J. Kunes, M. Svobodova, Substituted N-Phenylpyrazine-2-carboxamides: Synthesis and Antimycobacterial Evaluation. Molecules 14 (2009) 4180-4189.

[18] Gaussian 09, Revision B.01, M. J. Frisch, G. W. Trucks, H. B. Schlegel, G. E. Scuseria, M. A. Robb, J. R. Cheeseman, G. Scalmani, V. Barone, B. Mennucci, G. A. Petersson, H. Nakatsuji, M. Caricato, X. Li, H. P. Hratchian, A. F. Izmaylov, J. Bloino, G. Zheng,

J. L. Sonneberg, M. Hada, M. Ehara, K. Toyota, R. Fukuda, J. Hasegawa, M. Ishida, T. Nakajima, Y. Honda, O. Kitao, H. Nakai, T. Vreven, J. A. Montgomery, J. E. Peralta, F. Ogliaro, M. Bearpark, J. J. Heyd, E. Brothers, K. N. Kudin, V. N. Staroverov, T. Keith, R. Kobayashi, J. Normand, K. Raghavachari, A. Rendell, J. C. Knox, J. B. Cross, V. Bakken, C. Adamo, J. Jaramillo, R. Gomperts, R. E. Stratmann, O. Yazyev, A. J. Austin, R. Cammi, C. Pomelli, J. W. Ochterski, R. L. Martin, K. Morokuma, V. G. Zakrzewski, G. A. Voth, P. Salvador, J. J. Dannenberg, S. Dapprich, A. D. Daniels, O. Farkas, J. B. Foresman, J. V. Ortiz, J. Cioslowski, D. J. Fox, Gaussian Inc., Wallingford CT, 2010.

[19]   J. B. Foresman, A Guide to Using Gaussian, Pittsburg, PA, in E: Frisch (Ed.), Exploring Chemistry with Electronic Structure Methods, 1996.

[20]   J. M. L. Martin, C. Van Alsenoy, GAR2PED, A Program to obtain a potential energy distribution from a Gaussian archive record, University of Antwerp, Belgium, 2007.

[21]   R. Dennington, T. Keith, J. Millam, Gaussview, Version 5, Semichem Inc., Shawnee Missions KS, 2009.

[22]   A. D. Bochevarov, E. Harder, T. F. Hughes, J. R. Greenwood, D. A. Braden, D. M. Philipp, D. Rinaldo, M. D. Halls, J. Zhang, R. A. Friesner, Jaguar: a high-performance quantum chemistry software program with strengths in life and material sciences, Int. J. Quantum Chem. 113(18) (2013) 2110-2142.

[23]   D. Shivakumar, J. Williams, Y. Wu, W. Damm, J. Shelley, W. Sherman, prediction of absolute solvation free energies using molecular dynamics free energy perturbation and the OPLS force field, J. Chem. Theory Comput. 6(2010) 1509-1519.

[24]   J.L. Banks, H.S. Beard, Y. Cao, A.E. Cho, W. Damm, R. Farid, A.K. Felts, T.A. Halgren, D.T. Mainz, J.R. Maple, Integrated modeling program, applied chemical theory (IMPACT), J. Comput. Chem. 26 (16) (2005) 1752-1780.

[25]   Schrödinger Release 2015-4: Maestro, version 10.4, Schrödinger, LLC, New York, NY, 2015. 2015.

[26]   T. Joseph, H. T. Varghese, C. Y. Panicker, K. Viswanathan, M. Dolezal, C. Van Alsenoy, Spectroscopic (FT-IR, FT-Raman), first order hyperpolarizability, NBO analysis, HOMO and LUMO analysis of *N*-[(4-(trifluoromethyl)phenyl]pyrazine-2-carboxamide by density functional methods, Arabian J. Chem. 10 (S2) S2281-S2294.

[27]   W. He, G. Zhou, J. Li, A. Tian, Molecular design of analogues of 2,6-diamino-3,5-dinitropyrazine-1-oxide, J. Mol. Struct. THEOCHEM 668 (2004) 201-208.

[28]   N. P. G. Roeges, A Guide to the Complete Interpretation of Infrared Spectra of Organic Structures, Wiley, New York, 1994.

[29] N. B. Colthup, L. H. Daly, S. E. Wiberly, Introduction to infrared and Raman spectroscopy, Ed. 2, Academic Press, New York, 1975.

[30] G. Varsanyi, Assignments of Vibrational Spectra of Seven Hundred Benzene Derivatives, Wiley, New York 1974.

[31] Y. S. Mary, C. Y. Panicker, H. T. Varghese, K. Raju, T. E. Bolelli, I. Yildiz, C. M. Granadeiro, H. I. S. Nogueiro, Vibrational spectroscopic studies and computational study of 4-fluoro-*N*-(2'-hydroxy-4'-nitrophenyl) phenylacetamide, J. Mol. Struct. 994 (2011) 223-231.

[32] M. Barthes, G. De Nunzio, M. Ribet, Polarons or proton transfer in chains of peptide groups, Synth. Met. 76 (1996) 337-340.

[33] J. Lukose, C.Y. Panicker, P.S. Nayak, B. Narayana, B.K. Sarojini, C. Van Alsenoy, A. A. Al-Saadi, Synthesis, structural and vibrational investigation on 2-phenyl-*N*-(pyrazine-2-yl)acetamide combining XRD diffraction, FT-IR and NMR spectroscopies with DFT calculations, Spectrochim. Acta A 135 (2015) 608-616.

[34] E. Loh, Raman spectra of iodine derivatives of tyrosine and thyronine, J. Raman Spectrosc. 3 (1975) 327-333.

[35] R.A. Yadav, J. S. singh, O. Sala, The Raman and infrared spectra and normal coordinate analysis for 1,2-diiodotetraflurobenzene, J. Raman Spectrosc. 14 (1983) 353-357.

[36] D. A. Zainuri, S. Arshad, N. C. Khalib, I. A. Razak, R. R. Pillai, S. F. Sulaiman, N. S. Hashim, K. L. Ooi, S. Armaković, S. J. Armaković, C. Y. Panicker, synthesis, XRD crystal structure, spectroscopic characterization (FT-IR, 1H and 13C NMR), DFT studies, chemical reactivity and bond dissociation energy studies using molecular dynamics simulations and evaluation of antimicrobial and antioxidant activities of a novel chalcone derivative, (*E*)-1-(4-bromophenyl)-3-(4-iodophenyl)prop-2-en-1-one, J. Mol. Struct. 1128 (2017) 520-533.

[37] J. Coats, R. A. Meyers (Ed.), Encyclopedia of analytical chemistry, interpretation of Infrared spectra, a practical approach, in: John Wiley and Sons, Chichester, 2000.

[38] R. I. Al-Wabli, K. S. Resmi, Y. S. Mary, C. Y. Panicker, M. I. Attia, A. A. El-Emam, C. Van Alsenoy, Vibrational spectroscopic studies, Fukui functions, HOMO-LUMO, NLO, NBO analysis and molecular docking study of (*E*)-1-(1,3-benzodioxol-5-yl)-4,4-dimethylpent-1-en-3-one, a potential precursor to bioactive agents, J. Mol. Struct. 1123 (2016) 375-383.

[39] D. Philip, A. John, C.Y. Panicker, H.T. Varghese, FT-Raman, FT-IR and surface enhanced Raman scattering spectra of sodium salicylate, Spectrochim. Acta A 57 (2001) 1561-1566.

[40] J. F. Arenas, J. T. I. Navarrete, J. C. Ottero, J. I. Marcos, A. Cardenete, Vibrational spectra of [^{1}H$_4$] pyrazine and [^{2}H$_4$] pyrazine, J. Chem. Soc. Faraday Trans. 2 (81) (1985) 405-415.

[41] NBO Version 3.1, E.D. Glendening, A.E. Reed, J.E. Carpenter, F. Weinhold.

[42] M. Adant, M. Dupuis, J. L. Bredas, *Ab initio* study of the nonlinear optical properties of urea: Electron correlation and dispersion effects, Int. J. Quantum. Chem. 56 (1995) 497-507.

[43] A. S. El-Azab, Y. S. Mary, C. Y. Panicker, A. A.-M A-Aziz, A. Magda, El-Sherbeny, C. V. Alsenoy, DFT and experimental (FT-IR and FT-Raman) investigation of vibrational spectroscopy and molecular docking studies of 2-(4-oxo-3-phenyl-3,4-dihydroquinazolin-2-ylthio)-N-(3,4,5 trimethoxy phenyl) acetamide, J. Mol Struct. 1113 (2016) 133-145.

[44] F. J. Luque, J. M. Lopez, M. Orozco, Perspective on electrostatic interactions of a solute with a continuum, a direct utilization of ab initio molecular potentials for the prevision of solvent effects, Theor. Chem. Acc. 103 (2000) 343-345.

[45] P. Politzer, J. S. Murray, in: D. L. Beveridge, R. Lavery, (Eds.), Theoretical Biochemistry and Molecular Biophysics, Springer, Berlin, 1991.

[46] J.S. Murray, J.M. Seminario, P. Politzer, P. Sjoberg, Average local ionization energies computed on the surfaces of some strained molecules, Int. J. Quantum Chem. 38(S24) (1990) 645-653.

[47] P. Politzer, F. Abu-Awwad, J.S. Murray, Comparison of density functional and Hartree–Fock average local ionization energies on molecular surfaces, Int. J. Quantum Chem. 69(4) (1998) 607-613.

[48] A. Toro-Labb_e, P. Jaque, J.S. Murray, P. Politzer, Connection between the average local ionization energy and the Fukui function, Chem. Phys. Lett. 407(2005) 143-146.

[49] R.G. Parr, Density Functional Theory of Atoms and Molecules, in Horizons of Quantum Chemistry, Springer, (1980) 5-15.

[50] A. Michalak, F. De Proft, P. Geerlings, R. Nalewajski, Fukui functions from the relaxed Kohn-Sham orbitals, J. Phys. Chem. A 103 (1999) 762-771.

[51] X. Ren, Y. Sun, X. Fu, L. Zhu, Z. Cui, DFT comparison of the OH-initiated degradation mechanisms for five chlorophenoxy herbicides, J. Mol. Model. 19 (2013) 2249-2263.

[52]   l. Ai, J. Y. Liu, Mechanism of OH-initiated atmospheric oxidation of E/Z-CF3CF=
         CFCF3: a quantum mechanical study, J. Mol. Model. 20 (2014) 1-10.

[53]   W. Sang-aroon, V. Amornkitbamrung, V. Ruangpornvisuti, A density functional theory
         study on peptide bond cleavage at aspartic residues: direct vs cyclic intermediate
         hydrolysis, J. Mol. Model. 19 (2013) 5501-5513.

[54]   J. Kieffer, É. Brémond, P. Lienard, G. Boccardi, In silico assessment of drug substances
         chemical stability, J. Mol. Struct. THEOCHEM. 954 (2010) 75-79.

[55]   J.S. Wright, H. Shadnia, L.L. Chepelev, Stability of carbon-centered radicals: Effect of
         functional groups on the energetics of addition of molecular oxygen, J. Comput. Chem.
         30 (2009) 1016-1026.

[56]   P. Lienard, J. Gavartin, G. Boccardi, M. Meunier, Predicting drug substances
         autoxidation, Pharm. Res. 32(1) (2015) 300-310.

[57]   T. Andersson, A. Broo, E. Evertsson, Prediction of Drug Candidates' Sensitivity
         Toward Autoxidation: Computational Estimation of C☐ H Dissociation Energies of
         Carbon-Centered Radicals, J. Pharm. Sci. 103(7) (2014) 1949-1955.

[58]   R.V. Vaz, J.R. Gomes, C.M. Silva, Molecular dynamics simulation of diffusion
         coefficients and structural properties of ketones in supercritical CO 2 at infinite dilution,
         J. Supercritic. Fluids, 107 (2016) 630-638.

[59]   D.J. Greenhalgh, A.C. Williams, P. Timmins, P. York, Solubility parameters as
         predictors of miscibility in solid dispersions, J. Pharm. Sci. 88 (1999) 1182–1190.

[60]   R.C. Rowe, Adhesion of film coatings to tablet surfaces—a theoretical approach based
         on solubility parameters, Int. J. Pharm. 41 (1988) 219–222.

[61]   R.C. Rowe, Interactions in coloured powders and tablet formulations: a theoretical
         approach based on solubility parameters, Int. J. Pharm. 53 (1989) 47–51.

[62]   Lagunin, A.; Stepanchikova, A.; Filimonov, D.; Poroikov, V. "PASS: prediction of
         activity spectra for biologically active substances" Bioinformatics 16 (2000) 747-748.

[63]   F. Tsuji, H. Aono, Role of Transient Receptor Potential Vanilloid 1 in Inflammation and
         Autoimmune Diseases, Pharmaceuticals (Basel). 5 (8) (2012) 837-852.

[64]   F. Tsuji, M. Murai, K. Oki, Seki I, K. Ueda, H. Inoue, L. Nagelkerken, M. Sasano, H .
         Aono, Transient receptor potential vanilloid 1 agonists as candidates for anti-
         inflammatory and immunomodulatory agents., Eur. J. Pharmacol. 627 (2010) 332-339.

[65]   Y. K. C. D. Silva, C. V. Augusto, M. L. D. C. Barbosa, G. M. D. A. Melo, A. C. D.
         Queiroz, T. D. L. M. F. Dias, W. B. Júnior, E. J. Barreiro, L. M. Lima, M. S. A. Moreira,
         Synthesis and pharmacological evaluation of pyrazine N-acylhydrazone derivatives

designed as novel analgesic and anti-inflammatory drug candidates, Bioorganic and Medicinal Chemistry 18 (2010) 5007-5015.

[66] G. M. Morris, R. Huey, W. Lindstrom, M. F. Sanner, R. K. Belew, D. S. Goodsell, A. J. Olson, Autodock4 and AutoDockTools4: automated docking with selective receptor flexiblity. J. Computational Chemistry 16 (2009) 2785-2791.

[67] O. Trott, A. J. Olson, Auto Dock Vina: improving the speed and accuracy of docking with a new scoring function, efficient optimization and multi-threading J. Comput. Chem. 31 (2010) 455-461.

[68] G. M. Morris, D. S. Goodsell, R. S. Halliday, R. Huey, W. E. Hart, R. Belew, A. J. Olson, Automated docking using a Lamarckian genetic algorithm and an empirical binding free energy function, Journal of Computational Chemistry. 19 (1998) 1639-1662.

Figure Caption

Fig 1 FT-IR

Fig 2 FT-Raman

Fig 3 Molecule

Fig 4 HOMO-LUMO

Fig 5 MEP

Fig 6 ALIE

Fig 7 Fukui

Fig 8 BDE

Fig 9 RDF

Fig 10 Docking
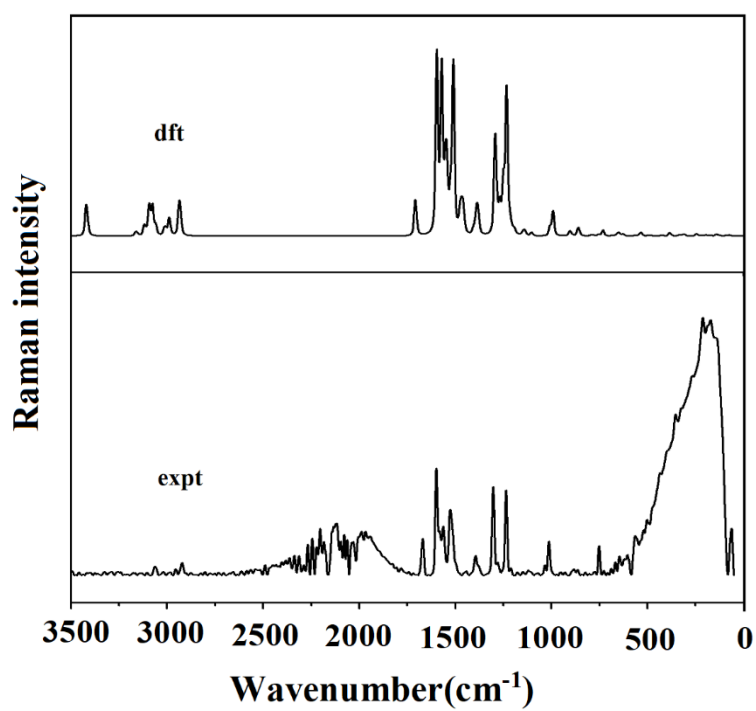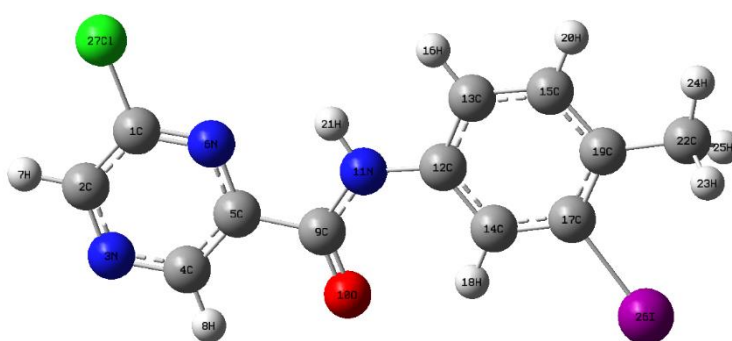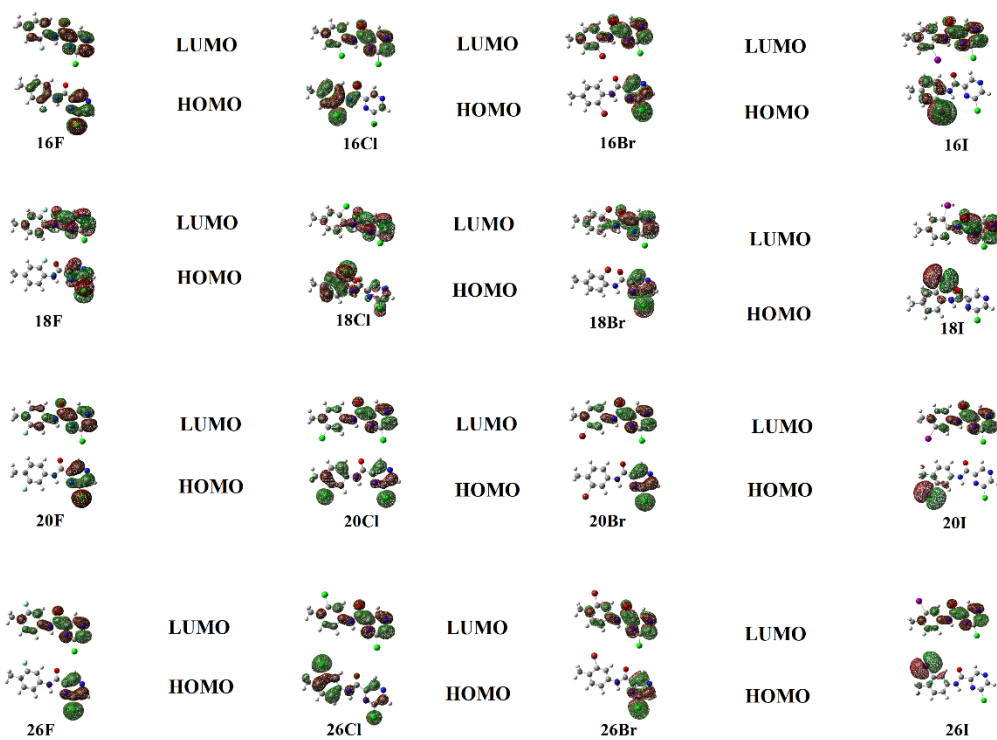
Fig 11 Docking

Table Caption

Graphical Abstract
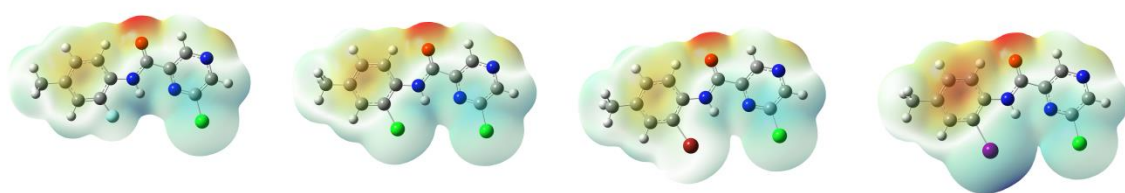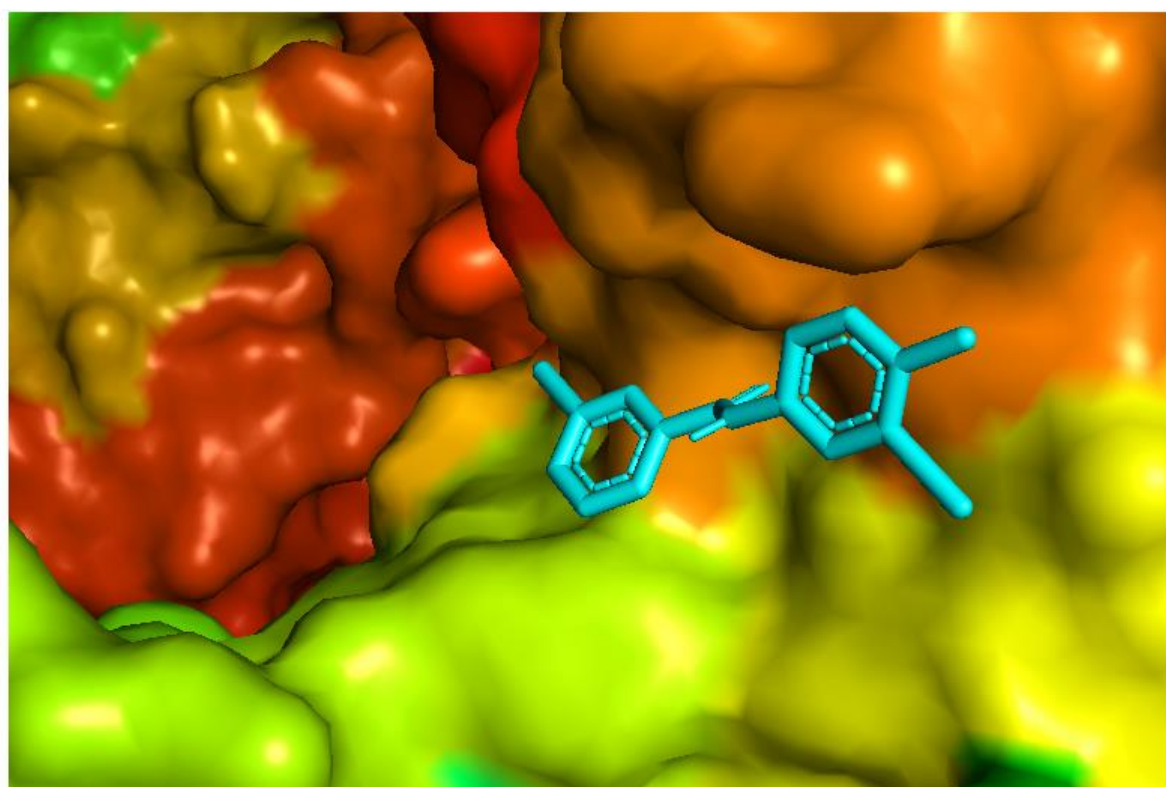
Figures
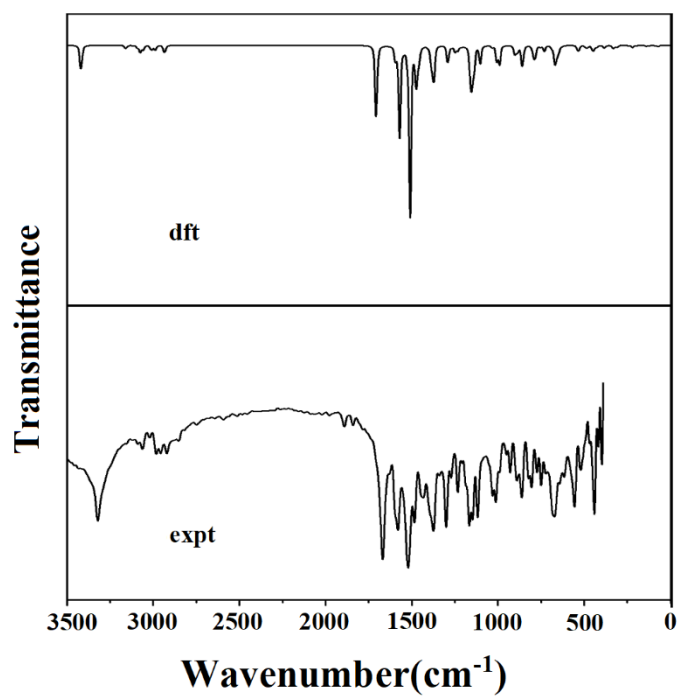
Fig. 1. FT-IR spectrum of CIMPPC

Fig. 2. FT-Raman spectrum of CIMPPC

Fig. 3. Optimized geometry of CIMPPC

LUMO HOMO 16F | LUMO HOMO 16Cl | LUMO HOMO 16Br | 16I
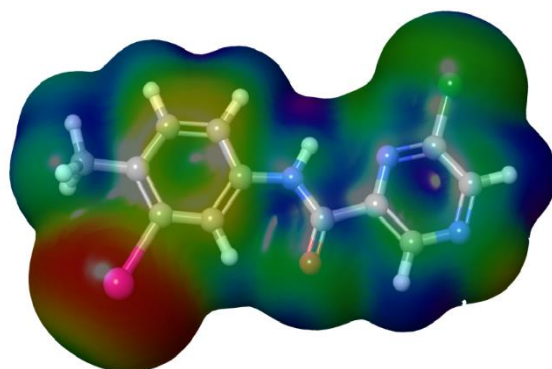
LUMO HOMO 18F | LUMO HOMO 18Cl | LUMO HOMO 18Br | 18I

LUMO HOMO 20F | LUMO HOMO 20Cl | LUMO HOMO 20Br | 20I

LUMO HOMO 26F | LUMO HOMO 26Cl | LUMO HOMO 26Br | 26I

Fig. 4. HOMO, LUMO plots of CIMPPC with halogen substitutions
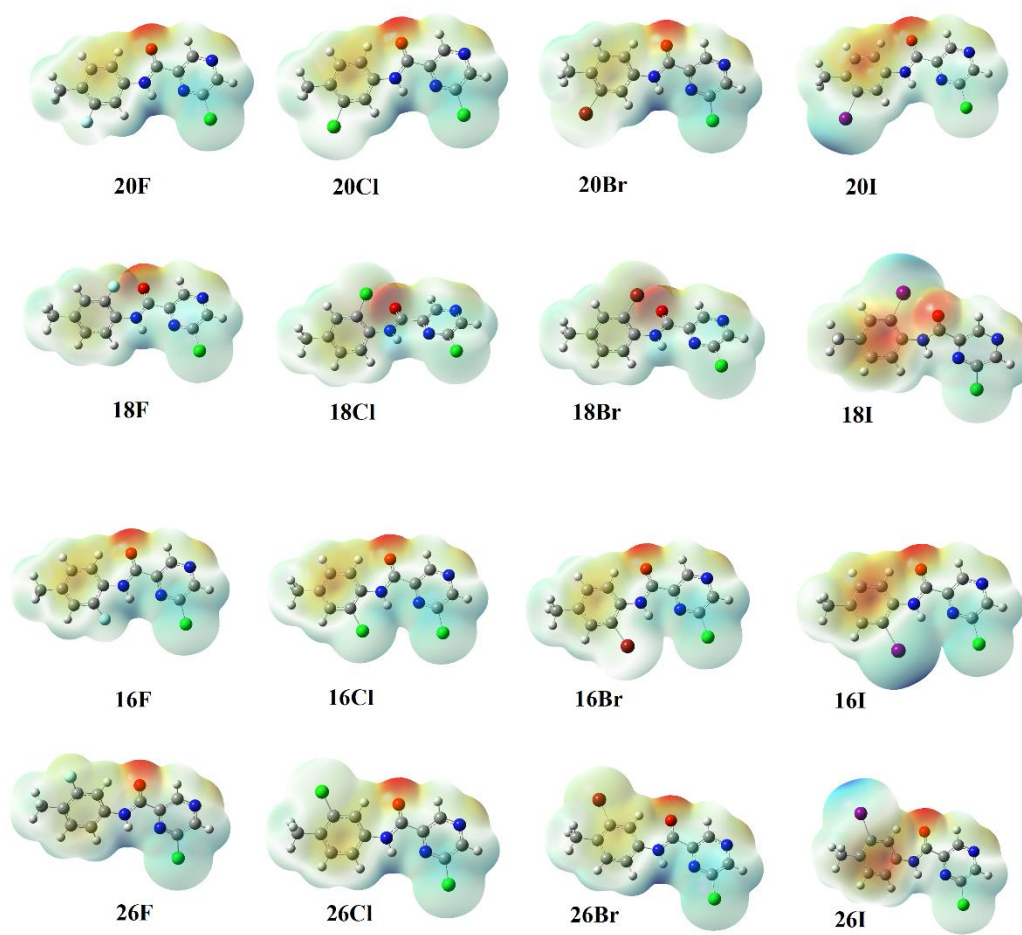
Fig. 5. MEP plots of CIMPPC with halogen substitutions

ALIE

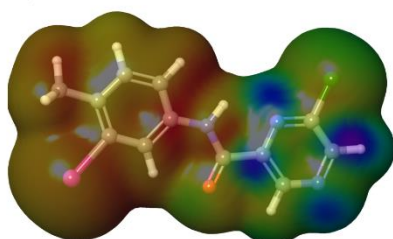**179.47 ALIE [Kcal/mol] 332.15**
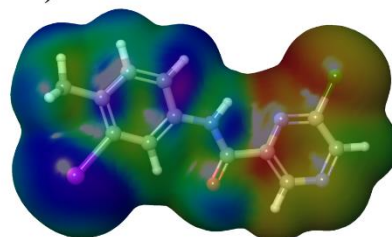
Fig. 6. ALIE surface of CIMPPC

f^+ f^-
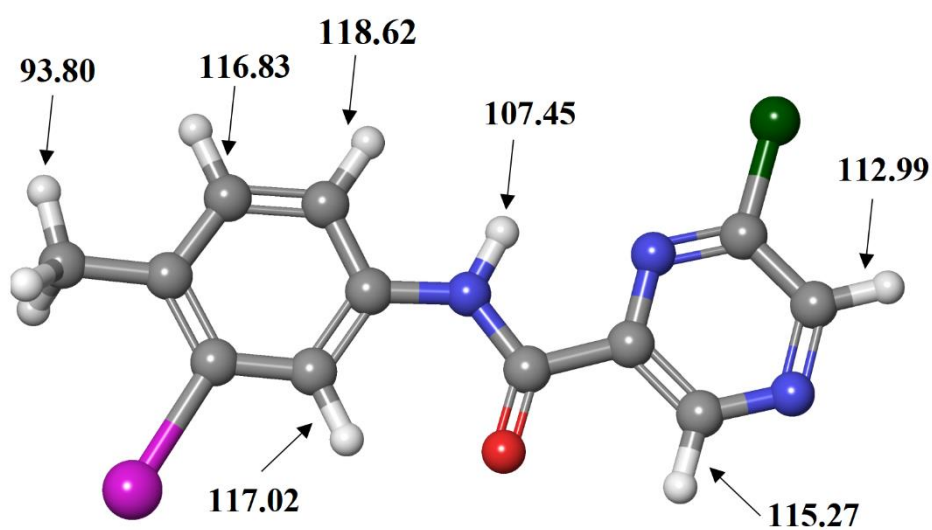
a)

-1.74 x 10^{-5} 5.36 x 10^{-4}

b)

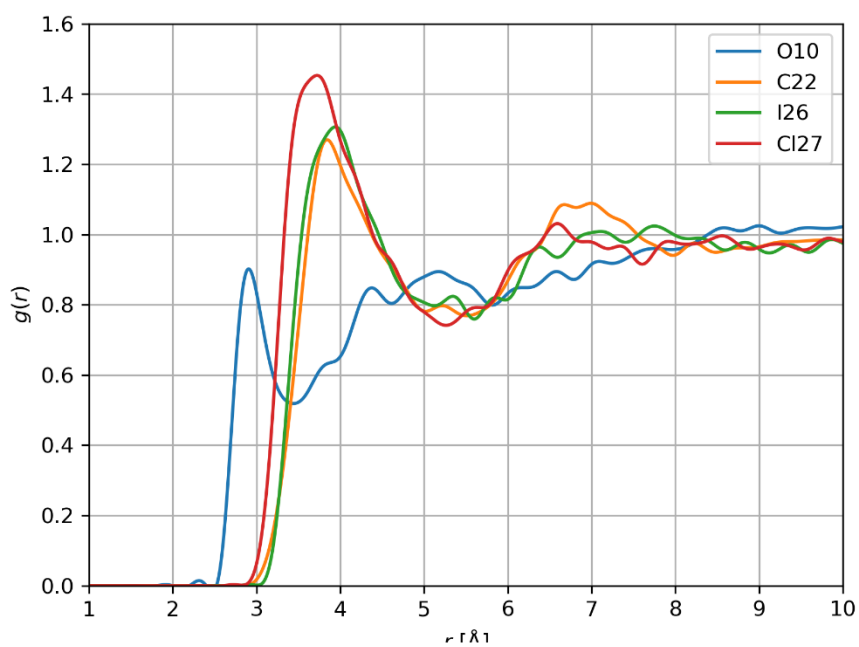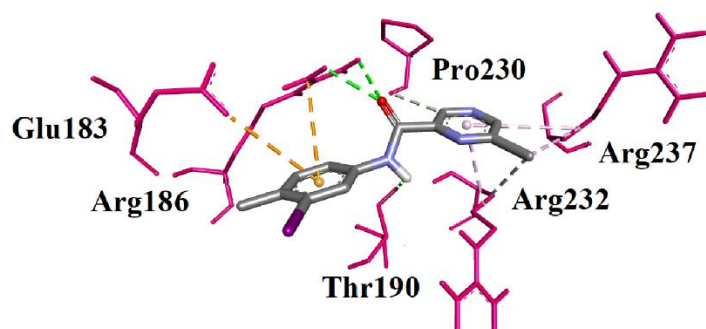**-2.68 x 10^{-5} 2.76 x 10^{-4}**

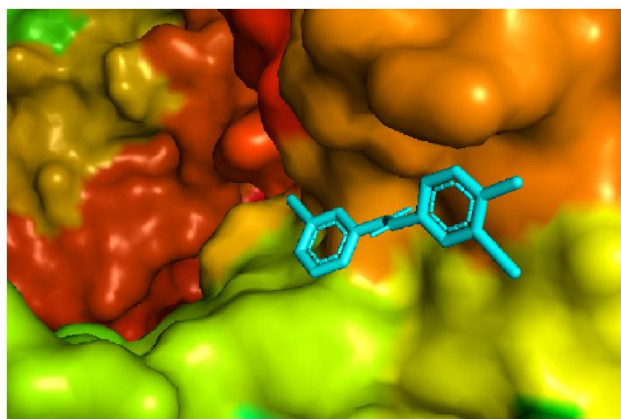## Fig. 7. Fukui functions a) f^+ and b) f^- of the CIMPPC

Fig. 8. BDEs of all single acyclic bonds of CIMPPC

Fig. 9. RDFs of CIMPPC atoms with significant interactions with water molecules

Fig. 10. Interactive plots of amino acids of the receptor with the ligand

Fig. 11. The docked ligand of CIMPPC at the active site of the receptor

Tables

Table 1

Optimized Geometrical parameters of 6-chloro-N-(3-iodo-4-methyl phenyl) pyrazine-2-carboxamide.

Bond length (Å)		Bond angles(°)		Dihedral angles(°)	
C_1-C_2	1.4038	C_2-C_1-N_6	122.4	N_6-C_1-C_2-C_3	0.0
C_1-N_6	1.3185	C_2-C_1-Cl_{27}	119.6	N_6-C_1-C_2-C_7	-180.0
C_1-Cl_{27}	1.7509	C_1-C_2-C_3	120.8	Cl_{27}-C_1-C_2-C_3	-180.0
C_2-N_3	1.3318	C_1-C_2-H_7	121.0	C_2-C_1-N_6-C_5	-0.0
C_2-H_7	1.0864	N_6-C_1-Cl_{27}	118.0	Cl_{27}-C_1-N_6-C_5	-180.0
N_3-C_4	1.3394	C_1-N_6-C_5	116.8	Cl_{27}-C_2-C_3-C_4	-0.0
C_4-C_5	1.3971	C_3-C_2-H_7	118.2	C_2-C_3-C_4-C_5	-0.0
C_4-H_8	1.0848	C_2-C_3-C_4	117.3	C_3-C_4-C_5-N_6	0.0
C_5-N_6	1.3440	C_3-C_4-C_5	121.5	C_3-C_4-C_5-C_9	-180.0
C_5-C_9	1.5094	C_3-C_4-H_8	118.2	C_4-C_5-N_6-Cl_{27}	-0.0
C_9-O_{10}	1.2267	C_5-C_4-H_8	120.3	C_9-C_5-N_6-C_1	180.0
C_9-N_{11}	1.3657	C_4-C_5-N_6	121.2	C_4-C_5-C_9-O_{10}	0.0
N_{11}-C_{12}	1.4074	C_4-C_5-C_9	120.0	C_4-C_5-C_9-N_{11}	-180.0
N_{11}-H_{21}	1.0152	N_6-C_5-C_9	118.8	N_6-C_5-C_9-O_{10}	-180.0
C_{12}-C_{13}	1.4014	C_5-C_9-O_{10}	120.5	N_6-C_5-C_9-N_{11}	0.0
C_{12}-C_{14}	1.4030	C_5-C_9-N_{11}	113.2	C_5-C_9-N_{11}-C_{12}	-180.0
C_{13}-C_{15}	1.3890	C_{10}-C_9-N_{11}	126.4	O_{10}-C_9-N_{11}-C_{12}	0.0
C_{13}-H_{16}	1.0875	C_9-N_{11}-C_{12}	128.8	C_9-N_{11}-C_{12}-C_{13}	180.0
C_{14}-C_{17}	1.3927	C_9-N_{11}-H_{21}	114.3	C_9-N_{11}-C_{12}-C_{14}	-0.0
C_{14}-H_{18}	1.0875	C_{12}-N_{11}-H_{21}	116.9	N_{11}-C_{12}-C_{13}-C_{15}	-180.0
C_{15}-C_{19}	1.4043	C_{11}-C_{12}-C_{13}	117.8	C_{14}-C_{12}-C_{13}-C_{15}	0.0
C_{15}-H_{20}	1.0869	C_{11}-C_{12}-C_{14}	122.9	N_{11}-C_{12}-C_{14}-C_{17}	180.0
C_{17}-C_{19}	1.4018	C_{13}-C_{12}-C_{14}	119.3	C_{13}-C_{12}-C_{14}-C_{17}	-0.0
C_{17}-I_{26}	2.1547	C_{12}-C_{13}-C_{15}	120.1	C_{12}-C_{13}-C_{15}-C_{19}	-0.0
C_{19}-C_{22}	1.5075	C_{12}-C_{13}-H_{16}	120.0	C_{12}-C_{14}-C_{17}-C_{19}	-0.0
C_{22}-H_{23}	1.0964	C_{12}-C_{14}-C_{17}	119.0	C_{12}-C_{14}-C_{17}-I_{26}	-180.0
C_{22}-H_{24}	1.0942	C_{12}-C_{14}-H_{18}	119.5	C_{13}-C_{15}-C_{19}-C_{17}	-0.0
C_{22}-H_{25}	1.0964	C_{15}-C_{13}-C_{16}	119.9	C_{13}-C_{15}-C_{19}-C_{22}	180.0
		C_{13}-C_{15}-C_{19}	122.4	C_{14}-C_{17}-C_{19}-C_{15}	0.0
		C_{13}-C_{15}-H_{20}	119.0	C_{14}-C_{17}-C_{19}-C_{22}	180.0
		C_{17}-C_{14}-H_{18}	121.6	I_{26}-C_{17}-C_{19}-C_{15}	180.0
		C_{14}-C_{17}-C_{19}	123.4	I_{26}-C_{17}-C_{19}-C_{22}	0.0
		C_{14}-C_{17}-I_{26}	116.4		
		C_{19}-C_{15}-H_{20}	118.6		
		C_{15}-C_{19}-C_{17}	115.9		
		C_{15}-C_{19}-C_{22}	120.2		
		C_{19}-C_{17}-I_{26}	120.2		
		C_{17}-C_{19}-C_{22}	123.9		
		C_{19}-C_{22}-H_{23}	111.5		

		C$_{19}$-C$_{22}$-H$_{24}$	110.6		
		C$_{19}$-C$_{22}$-H$_{25}$	111.5		
		H$_{23}$-C$_{22}$-H$_{24}$	108.1		
		H$_{23}$-C$_{22}$-H$_{25}$	106.8		
		H$_{24}$-C$_{22}$-H$_{25}$	108.1		

Table 2

Calculated scaled wavenumbers, observed IR, Raman bands and vibrational assignments with potential energy distribution (PED) of the title compound.

B3LYP/gen				IR(cm^{-1})	Raman(cm^{-1})	Assignments[a]
ν(cm^{-1})[b]	ν(cm^{-1})[c]	IR$_I$	R$_A$			
3556	3418	76.90	247.15	3330	3494	νNH(91)
3286	3159	10.23	29.34	-	-	νCHPh(99)
3241	3116	0.48	70.55	-	-	νCHPz(99)
3217	3093	4.95	146.37	-	-	νCHPz(99)
3200	3077	17.56	159.69	-	-	νCHPh(99)
3182	3059	11.72	51.55	3062	3063	νCHPh(99)
3131	3010	16.98	72.38	3024	-	νCH$_3$(79)
3107	2987	12.08	99.59	2982	2957	νCH$_3$(78)
3052	2934	24.50	261.06	2925	2924	νCH$_3$(93)
1775	1706	198.96	153.36	1670	1667	νCO(66)
1660	1596	29.42	617.65	1580	1598	νPh(54), δCHPh(14)
1635	1571	239.88	635.27	-	1561	νPh(42), δNH(15)
1610	1548	11.57	477.37	-	-	νPz(69), δCHPz(19)
1584	1523	38.45	203.67	1520	1525	νPz(75)
1570	1509	391.56	550.79	-	-	δNH(34), νPh(27)
1536	1476	95.98	74.90	1485	-	νPh(39), νCHPh(31)
1521	1462	64.19	173.43	-	-	δCH$_3$(75)
1512	1453	6.12	19.35	1433	-	δCH$_3$(95)
1463	1406	2.18	17.01	-	1395	νPz(41), δCHPz(28)
1449	1392	1.03	33.04	1377	-	δCH$_3$(62), νC$_{19}$C$_{22}$(19)
1440	1384	70.36	153.67	-	-	δCHPz(43), νPz(14), νPh(10)
1428	1373	83.38	1.72	-	-	νPh(26), δCHPz(22), νCHPh(16)
1343	1291	51.05	422.73	1298	1302	νPh(69)
1320	1269	3.80	100.71	-	-	δCHPh(39)
1298	1248	17.99	199.57	-	-	δCHPh(25), νC$_5$C$_9$(17), νPz(13)
1281	1232	9.95	458.13	1230	1237	νCN(28), νPh(21), δCN(14)
1261	1212	4.22	46.39	-	-	νPz(81)
1241	1193	2.75	26.02	1166	1179	δCHPh(29), νPh(13), δPh(11)
1204	1158	139.97	3.37	1147	-	δCHPz(36), νPz(34), δPz(13), νPh(11)
1191	1145	29.06	6.05	-	-	νPz(27), δCHPh(22)
1186	1140	59.64	19.73	1121	1118	νPz(24), δCHPh(22), δCHPz(17)

1148	1103	42.21	9.99	-	-	νCN(26), νPz(22)
1075	1033	4.17	0.19	1031	1035	δCH$_3$(89)
1047	1007	35.55	23.23	1009	1015	δPh(43), νPh(27)
1031	991	42.31	70.72	-	-	νPz(62), δPz(55)
1029	989	3.85	9.31	-	-	δCH$_3$(70)
981	943	0.89	1.42	-	958	γCHPz(88)
945	908	0.75	2.02	926	-	γCHPh(91)
938	902	21.17	16.0	889	886	δCN(21), νC$_9$C$_5$(16), δPz(13), νCCl(11)
926	890	14.86	1.18	-	-	γCHPh(79)
919	884	8.28	0.06	-	-	γCHPz(73)
892	858	62.66	32.03	862	866	νPh(21), δPh(15)
826	794	29.54	3.18	-	-	γCHPh(79)
817	785	27.42	2.56	776	-	δCO(20), δPz(20)
784	753	4.92	5.54	749	749	δPz(39), γC$_5$C$_9$(27), γCO(27)
761	732	13.78	16.72	723	-	δPh(23), νC$_{19}$C$_{22}$(23), δPz(10)
735	707	0.44	0.20	-	-	γPz(56), δCO(17)
712	685	8.56	1.35	-	691	γPh(74)
694	667	63.76	1.63	674	668	γNH(44), γCO(29)
676	650	25.67	14.45	644	648	δPh(70)
654	629	1.18	6.23	614	603	δPz(66)
584	562	0.03	2.34	550	566	γPh(30), γC$_{19}$C9$_{22}$(12)
556	535	20.34	14.29	516	504	γCO(28), δPh(22)
518	498	1.25	0.95	-	-	γCCl(35), γPz(24), γCO(10)
504	485	9.43	2.57	-	-	δPh(27), δPz(26), νC$_9$C$_5$(12)
467	449	20.88	0.24	441	435	γPz(63), γC$_5$C$_9$(15)
447	430	4.74	0.67	-	-	γPh(62)
440	423	0.74	1.92	396	-	δC$_{19}$C$_{22}$(35), δCN(16)
398	383	7.11	8.94	366	-	νCCl(39), δPz(18)
351	337	0.49	2.24	357	354	γC$_{19}$C$_{22}$(35), γPh(25)
344	330	9.25	1.33	-	-	γCO(36), δCN(23)
323	311	6.34	7.57	-	271	νCI(30), δCCl(26)
254	244	0.89	6.23	-	-	δPh(18), νC$_5$C$_9$(11)
230	221	5.28	1.22	-	211	νCI(33), δCCl(23)
207	199	0.55	1.20	-	-	γCI(16), γCN(14), τPh(13), τCO(12)
204	196	0.49	1.98	-	-	δCI(41), δC$_{19}$C$_{22}$(15)
179	172	0.04	1.88	-	168	τPz(69), γCCl(16)
164	157	0.03	0.00	-	-	τCH$_3$(86)
147	142	1.83	3.94	-	-	γCI(24), γC$_5$C$_9$(19), τPh(13)
132	127	1.47	1.80	-	-	τPh(48), τCN(14)
90	87	1.39	3.03	-	-	δC$_5$C$_9$(28), τCI(27), τCN(14)
74	72	2.89	1.76	-	-	τC$_5$C$_9$(50), τCN(27), τPh(11)
51	49	0.15	0.03	-	-	τCO(40), τC$_5$C$_9$(15), τCN(14)
36	35	0.64	0.01	-	-	τCO(37), τCN(27)
19	18	0.00	0.11	-	-	τCN(63), τCO(16)

[a] ν-stretching; δ-in-plane deformation; γ-out-of-plane deformation; τ-torsion;
Ph-C$_{12}$-C$_{13}$-C$_{15}$-C$_{19}$-C$_{17}$-C$_{14}$; Pz-C$_1$-C$_2$-N$_3$-C$_4$-C$_5$-N$_6$.
[b] Unscaled wavenumber.
[c] Scaled wavenumber.

Table 3

Second-order perturbation theory analysis of Fock matrix in NBO basis corresponding to the intramolecular bonds of the title compound.

Donor(i)	type	ED/e	Acceptor(j)	Type	ED/e	$E(2)^a$	$E(j)-E(i)^b$	$F(ij)^c$
C_1-N_6	σ	1.98582	C_1-C_2	σ*	0.05017	0.89	1.36	0.031
-	π	1.73005)	C_2-N_3	π*	0.32058	18.49	0.31	0.069
-	π	-	C_4-C_5	π*	0.04365	20.70	0.33	0.075
C_2-N_3	π	1.70809	C_1-N_6	π*	0.38561	20.02	0.29	0.069
-	π	-	C_4-C_5	π*	0.29757	22.45	0.32	0.075
C_4-C_5	σ	1.98640	C_1-N_6	σ*	0.03033	0.61	1.21	0.024
-	π	1.62140	C_1-N_6	π*	0.38561	20.47	0.26	0.065
-	π	-	C_2-N_3	π*	0.32058	19.14	0.27	0.065
-	π	-	C_9-O_{10}	π*	0.28710	10.70	0.31	0.053
$C_{12}-C_{13}$	σ	1.97164	$N_{11}-C_{12}$	σ*	0.03414	0.87	1.06	0.027
-	π	1.63542	$C_{14}-C_{17}$	π*	0.39086	22.68	0.27	0.070
-	π	-	$C_{15}-C_{19}$	π*	0.34201	20.85	0.29	0.070
$C_{14}-C_{17}$	σ	1.97706	$N_{11}-C_{12}$	σ*	0.03414	4.21	1.08	0.060
-	π	1.72017	$C_{12}-C_{13}$	π*	0.38599	18.51	0.30	0.068
-	π	-	$C_{15}-C_{19}$	π*	0.34201	19.17	0.31	0.070
$C_{15}-C_{19}$	π	1.63333	$C_{12}-C_{13}$	π*	0.38599	22.77	0.27	0.070
-	π	-	$C_{14}-C_{17}$	π*	0.39086	23.23	0.26	0.070
LPN_3	σ	1.92158	C_1-C_2	σ*	0.05017	11.01	0.82	0.085
LPN_3	σ	-	C_4-C_5	σ*	0.04365	10.63	0.84	0.085
LPN_6	σ	1.89228	C_1-C_2	σ*	0.05017	11.12	0.81	0.086
LPN_6	σ	-	C_4-C_5	σ*	0.04365	10.21	0.83	0.084
LPO_{10}	π	-	C_5-C_9	σ*	0.07420	18.84	0.62	0.098
LPO_{10}	π	-	C_9-N_{11}	σ*	0.07354	22.46	0.65	0.109
LPN_{11}	σ	-	C_9-O_{10}	π*	0.28710	50.74	0.29	0.109
LPN_{11}	σ	-	$C_{12}-C_{13}$	π*	0.38599	31.00	0.31	0.088
$LPCl_{27}$	n	1.91841	C_1-N_6	π*	0.38561	14.26	0.27	0.060

Table 4

NBO results showing the formation of Lewis and non-Lewis orbitals of title compound.

Bond(A-B)	ED/ea	EDA%	EDB%	NBO	s%	p%
$σC_1-C_2$	1.99140	50.76	49.24	$0.7125(sp^{1.40})C$	41.67	58.33
-	-0.78221	-	-	$+0.7017(sp^{1.77})C$	36.14	63.86
$σC_1-N_6$	1.98582	39.57	60.43	$0.6290(sp^{1.87})C$	34.86	65.14
-	-0.98582	-	-	$+0.7774(sp^{1.75})N$	36.41	63.59
$πC_1-N_6$	1.73005	45.46	54.54	$0.6742(sp^{1.00})C$	0.00	100.00
-	-0.36803	-	-	$+0.7385(sp^{1.00})N$	0.00	100.00
$σC_1-Cl_{27}$	1.98115	43.96	56.04	$0.6630(sp^{3.28})C$	23.38	76.62
-	-0.70944	-	-	$+0.7486(sp^{5.94})C$	14.42	85.58
$σC_2-N_3$	1.98229	40.06	59.94	$0.6329(sp^{2.18})C$	31.47	68.53
-	--0.34997	-	-	$+0.7742(sp^{1.90})N$	34.49	65.51
$πC_2-N_3$	1.70809	42.91	57.09	$0.6551(sp^{1.00})C$	0.00	100.00

-	-0.87490	-	-	+0.7556(sp$^{1.00}$)N	0.00	100.00
σN$_3$-C$_4$	1.98489	59.97	40.03	0.7744(sp$^{1.90}$)N	34.45	65.55
-	-0.86687	-	-	+0.6327(sp2.24)C	30.82	69.18
σC$_4$-C$_5$	1.98640	49.27	50.73	0.7019(sp$^{1.69}$)C	37.19	62.81
-	-0.76925	-	-	+0.7122(sp$^{1.70}$)C	37.09	62.91
πC$_4$-C$_5$	1.62140	49.06	50.94	0.7004(sp$^{1.00}$)C	0.01	99.99
-	-0.31939	-	-	+0.7137(sp$^{99.99}$)C	0.01	99.99
σC$_5$-N$_6$	1.97150	39.88	60.12	0.6315(sp$^{2.28}$)C	30.46	69.54
-	-0.87076	-	-	+0.7754(sp$^{1.86}$)N	34.96	65.04
σC$_5$-C$_9$	1.96638	52.10	47.90	0.7218(sp$^{2.08}$)C	32.43	67.57
-	-0.69127	-	-	+0.6921(sp$^{1.91}$)C	34.35	65.65
σC$_9$-O$_{10}$	1.98952	34.60	65.40	0.5883(sp$^{2.13}$)C	31.90	68.10
-	-1.00167	-	-	+0.8087(sp$^{1.97}$)O	33.67	66.33
πC$_9$-O$_{10}$	1.97656	32.17	67.83	0.5672(sp$^{55.54}$)C	1.77	98.23
-	-0.42140	-	-	+0.8236(sp$^{54.69}$)O	1.80	98.20
σC$_9$-N$_{11}$	1.98598	36.36	63.64	0.6030(sp$^{2.12}$)C	32.03	67.97
-	-0.85300	-	-	+0.7978(sp$^{1.78}$)N	35.92	64.08
σN$_{11}$-C$_{12}$	1.98280	63.01	36.99	0.7938(sp$^{1.69}$)N	37.19	62.81
-	-0.81409	-	-	+0.6082(sp$^{2.68}$)C	27.16	72.84
σC$_{12}$-C$_{13}$	1.97164	51.28	48.72	0.7161(sp1.68)C	37.34	62.66
-	-0.70877	-	-	+0.6980(sp$^{1.96}$)C	33.79	66.21
πC$_{12}$-C$_{13}$	1.63542	51.24	48.76	0.758(sp$^{1.00}$)C	0.00	100.00
-	-0.26987	-	-	+0.6983(sp$^{1.00}$)C	0.00	100.00
σC$_{12}$-C$_{14}$	1.96297	50.28	49.72	0.7091(sp$^{1.82}$)C	35.41	64.59
-	-0.71281	-	-	+0.7051(sp$^{1.83}$)C	35.35	64.65
σC$_{13}$-C$_{15}$	1.97541	50.06	49.94	0.7075(sp$^{1.80}$)C	35.73	64.27
-	-0.69942	-	-	+0.7067(sp$^{1.80}$)C	35.67	64.33
σC$_{14}$-C$_{17}$	1.97706	50.02	49.98	0.7072(sp$^{1.74}$)C	36.45	63.55
-	-0.73587	-	-	+0.7070(sp$^{1.53}$)C	39.45	60.55
πC$_{14}$-C$_{17}$	1.72017	48.11	51.89	0.6936(sp$^{1.00}$)C	0.00	100.00
-	-0.28552	-	-	+0.7203(sp$^{1.00}$)C	0.00	100.00
σC$_{15}$-C$_{19}$	1.96170	49.31	50.69	0.7022(sp$^{1.77}$)C	36.11	63.89
-	-0.69504	-	-	+0.7120(sp$^{1.93}$)C	34.07	65.93
πC$_{15}$-C$_{19}$	1.63333	49.99	50.01	0.7070(sp$^{1.00}$)C	0.00	100.00
-	-0.25852	-	-	+0.7072(sp$^{1.00}$)C	0.00	100.00
σC$_{17}$-C$_{19}$	1.97709	50.40	49.60	0.7100(sp$^{1.43}$)C	41.11	58.89
-	-0.72842	-	-	+0.7042(sp$^{1.94}$)C	34.01	65.99
σC$_{17}$-I$_{26}$	1.97175	53.77	46.23	0.7333(sp$^{4.06}$)C	19.78	80.22
-	-0.49972	-	-	+0.6799(sp$^{8.65}$)C	10.37	89.63
σC$_{19}$-C$_{22}$	1.97831	50.95	49.09	0.7138(sp$^{2.14}$)C	31.89	68.11
-	-0.63165	-	-	+0.7004(sp$^{2.35}$)C	29.84	70.16
n1N$_3$	1.92158	-	-	Sp2.21	31.11	68.89
-	-0.38057			-	-	-
n1N$_6$	1.89228	-	-	Sp2.49	28.68	71.32
-	-0.37174			-	-	-
n1O$_{10}$	1.97545	-	-	Sp0.55	64.52	35.48
-	-0.70487			-	-	-
n2O$_{10}$	1.87439	-	-	Sp99.99	0.06	99.94
-	-0.27662			-	-	-

n1N$_{11}$ -	1.65763 -0.29824	-	-	Sp99.99 -	0.07 -	99.93 -
1I$_{26}$ -	1.99300 -0.61887	-	-	Sp0.12 -	89.54 -	10.46 -
n2I$_{26}$ -	1.97743 -0.27418	-	-	Sp99.99 -	0.14 -	99.86 -
n3I$_{26}$ -	1.95066 -0.27235	-	-	Sp0.17 -	0.00 -	100.00 -
n1Cl$_{27}$ -	1.99197 -0.94724	-	-	Sp0.17 -	85.15 -	14.85 -
n2Cl$_{27}$ -	1.97091 -0.33659	-	-	Sp99.99 -	0.44 -	99.56 -
n3Cl$_{27}$ -	1.91841 -0.33348	-	-	Sp1.00 -	0.00 -	100.00 -

Table 5

Polarizability values of CIMPPC with halogen substitutions

	μ debye	α x 10^{-23}esu	β x 10^{-30} esu	γ x10^{-37} esu
26I	3.5147	2.782	24.973	-21.240
26Br	3.3623	2.756	25.460	-19.876
26Cl	3.5352	2.671	24.853	-18.287
26F	3.0499	2.500	26.287	-15.968
16I	1.6246	2.790	32.504	-17.348
16Br	1.1896	2.727	21.866	-16.345
16Cl	1.1041	2.650	21.835	-15.686
16F	1.3843	2.503	24.355	-14.868
18I	1.7722	1.795	5.402	-17.668
18Br	2.9675	2.605	36.782	-16.441
18Cl	3.1251	2.527	3.269	-15.783
18F	2.8580	2.409	8.735	-14.933
20I	0.7531	2.845	38.874	-21.595
20Br	0.8064	2.756	26.477	-19.683
20Cl	0.7935	2.671	25.702	-18.086
20F	0.9418	2.500	26.808	-15.878

Table 6

HOMO, LUMO and Chemical descriptors of CIMPPC with halogen substitutions

	HOMO	LUMO	I = -E$_{HOMO}$	A = -E$_{LUMO}$	Gap	η = (I-A)/2	μ = (I+A)/2	ω = μ^2/2η
26I	-0.21808	-0.18744	5.934	5.100	0.834	0.417	-5.517	36.496
26Br	-0.29757	-0.18747	8.097	5.101	2.996	1.498	-6.599	14.535
26Cl	-0.29652	-0.18722	8.069	5.094	2.975	1.488	-6.582	14.557
26F	-0.29755	-0.18727	8.097	5.096	3.001	1.501	-6.597	14.497
16I	-0.22020	-0.18879	5.992	5.137	0.885	0.428	-5.565	36.179

16Br	-0.29750	-0.18761	8.095	5.105	2.990	1.495	-6.600	14.569
16Cl	-0.28821	-0.18699	7.842	5.088	2.754	1.377	-6.465	15.177
16F	-0.29707	-0.18725	8.084	5.095	2.989	1.495	-6.590	14.524
18I	-0.21454	-0.18622	5.838	5.067	0.771	0.386	-5.453	38.517
18Br	-0.29766	-0.18473	8.100	5.027	3.073	1.537	-6.564	14.016
18Cl	-0.29480	-0.18431	8.021	5.015	3.006	1.503	-6.518	14.133
18F	-0.29757	-0.18523	8.097	5.040	3.057	1.529	-6.569	14.111
20I	-0.21820	-0.18876	5.937	5.136	0.801	0.401	-5.537	38.227
20Br	-0.29756	-0.18742	8.097	5.100	2.997	1.499	-6.599	14.525
20Cl	-0.29713	-0.18705	8.085	5.090	2.995	1.498	-6.588	14.487
20F	-0.29754	-0.18709	8.096	5.091	3.005	1.503	-6.594	14.465

Table 7

Values of solubility parameters δ [MPa$^{1/2}$] for studied molecules and the excipient

Molecules	δ [MPa$^{1/2}$]
CIMPPC	23.426
PVP	18.515
Maltose	28.564
Sorbitol	32.425

Table 8

PASS prediction for the activity spectrum of CIMPPC compound. Pa represents probability to be active and Pi represents probability to be inactive.

Pa	Pi	Activity
0.708	0.003	Vanilloid 1 agonist
0.675	0.078	Ubiquinol-cytochrome-c reductase inhibitor
0.477	0.003	Vanilloid agonist
0.431	0.056	Platelet derived growth factor receptor kinase inhibitor
0.370	0.007	Lymphocytopoiesis inhibitor
0.408	0.083	Erythropoiesis stimulant
0.466	0.142	Nicotinic alpha6beta3beta4alpha5 receptor antagonist
0.350	0.027	Imidazoline I1 receptor agonist
0.363	0.050	CF transmembrane conductance regulator agonist
0.335	0.038	Antineoplastic (pancreatic cancer)
0.324	0.030	Thyroxine 5-deiodinase inhibitor
0.374	0.085	Peptide agonist
0.364	0.076	Centromere associated protein inhibitor
0.316	0.037	Thiamine pyridinylase inhibitor

0.352 0.074 Autoimmune disorders treatment
0.362 0.093 5 Hydroxytryptamine release inhibitor
0.302 0.037 Antihelmintic
0.284 0.022 Pancreatic disorders treatment
0.352 0.095 RNA-directed RNA polymerase inhibitor
0.317 0.062 Antituberculosic
0.276 0.023 Blasticidin-S deaminase inhibitor
0.285 0.038 Sodium channel blocker
0.296 0.057 Antiparasitic
0.235 0.003 Sodiumhydrogen exchanger 5 inhibitor
0.362 0.143 Nicotinic alpha2beta2 receptor antagonist
0.236 0.023 Aurora-C kinase inhibitor
0.231 0.018 Complement inhibitor

Table 9

The binding affinity values of different poses of the compound CIMPPC predicted by Autodock Vina.

Mode	Affinity (kcal/mol)	Distance from best mode (Å)	
		RMSD l.b.	RMSD u.b.
1	-5.9	0.000	0.000
2	-5.7	1.649	2.135
3	-5.6	18.110	20.686
4	-5.4	3.679	6.984
5	-5.4	17.560	19.338
6	-5.3	17.033	18.815
7	-5.3	17.397	19.392
8	-5.3	12.883	15.474
9	-5.3	3.992	7.341